

Quantum chaos challenges many-body localization

Jan Šuntajs,¹ Janez Bonča,^{2,1} Tomaž Prosen,² and Lev Vidmar¹

¹*Department of Theoretical Physics, J. Stefan Institute, SI-1000 Ljubljana, Slovenia*

²*Department of Physics, University of Ljubljana, SI-1000 Ljubljana, Slovenia*

Characterizing states of matter through the lens of their ergodic properties is a fascinating new direction of research. In the quantum realm, the many-body localization (MBL) [1, 2] was proposed to be the paradigmatic nonergodic phenomenon, which extends the concept of Anderson localization [3] to interacting systems. At the same time, random matrix theory has established a powerful framework for characterizing the onset of quantum chaos and ergodicity (or the absence thereof) in quantum many-body systems [4]. Here we study a paradigmatic class of models that are expected to exhibit MBL, i.e., disordered spin chains with Heisenberg-like interactions. Surprisingly, we observe that exact calculations show no evidence of approaching MBL while increasing disorder strength in the ergodic regime. Moreover, a scaling analysis suggests that quantum chaotic properties survive for any disorder strength in the thermodynamic limit. Our results are based on calculations of the spectral form factor, which provides a powerful measure for the emergence of many-body quantum chaos.

Quantum many-body physics is currently facing a revival in addressing long-standing open questions, such as the emergence of quantum ergodicity in nonequilibrium interacting systems. An extensive amount of recent theoretical and experimental work [4, 5] established a general view that, in the absence of disorder, generic quantum many-body systems are quantum ergodic in the sense that they thermalize after being driven away from equilibrium. The cornerstone of our understanding of thermalization is the eigenstate thermalization hypothesis [4], which claims that the knowledge of a single typical eigenstate is enough to predict expectation values of observables at long times after equilibration.

It is understood that foundations of the eigenstate thermalization hypothesis are based on the random matrix theory (RMT) [4]. Since the quantum chaos conjecture put forward in the 1980's [6–8], the RMT has been used as a key indicator of quantum chaos in isolated quantum systems. In recent years, the focus

has shifted towards many-body quantum chaos and its manifestations in different fields of physics, ranging from models relevant for holographic duality [9–12] to lattice models in condensed matter [13–16]. In the later case, the emergence of the RMT statistics was rigorously proved in a periodically kicked Ising chain [16].

MBL was proposed as a phase of matter emerging in strongly disordered quantum many-body lattice systems with local interactions [1, 2]. Such a state is an ideal insulator, i.e., insulator at arbitrary temperature. As one of the hallmark features of MBL, it is considered that the spectra of systems exhibiting MBL do not obey the RMT statistics [2, 17] and

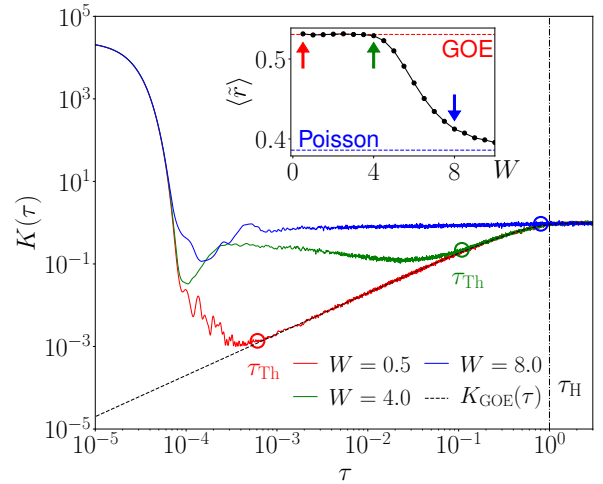


FIG. 1. SFF $K(\tau)$ in the disordered spin chain. Results are shown for the anisotropic J_1 - J_2 chain at three disorder strengths W (as indicated in the legend) on a lattice with $L = 18$ sites. The black dashed line is the GOE prediction $K_{GOE}(\tau)$. Open circles denote the scaled Thouless time τ_{Th} and the vertical line denotes the scaled Heisenberg time $\tau_H \equiv 1$. In the inset we show the average level spacing ratio $\langle \tilde{r} \rangle$ [see Methods for the definition of $\langle \tilde{r} \rangle$]. The arrows are located at values of W used in the main panel. The horizontal lines in the inset denote the GOE prediction $\tilde{r}_{GOE} \approx 0.5307$ and the prediction for energy levels with Poisson statistics $\tilde{r}_{Poisson} \approx 0.3863$.

hence quantum chaos is expected to be absent at large enough disorder. The existence of MBL has not yet been rigorously proved. Yet, the majority of previous works were interpreted in the framework of a stable MBL phase in one dimension at strong disorder [18–24], consistent with careful analytic perturbative arguments that support existence of MBL [20–22]. However, the stability of MBL has been questioned in other systems, such as disordered spin chains coupled to a small bath [25], the interacting Aubry-Andree-Harper model [26], and two-dimensional systems [27].

Here we study the scaling of spectral properties in a class of generic spin chains, which were believed to exhibit MBL. We focus on one of the most universal and versatile tools for the analysis of spectral properties, i.e., a Fourier transform of the two-point correlations, known as the spectral form factor (SFF). It is defined as

$$K(\tau) = \frac{1}{Z} \left\langle \left| \sum_{\alpha=1}^{\mathcal{D}} g(\varepsilon_{\alpha}) e^{-i\varepsilon_{\alpha}\tau} \right|^2 \right\rangle, \quad (1)$$

where $\{\varepsilon_1 \leq \varepsilon_2 \leq \dots \varepsilon_{\mathcal{D}}\}$ is the complete set of Hamiltonian eigenvalues, \mathcal{D} is the Hilbert space dimension, and the normalization Z is such that $K(\tau \gg 1) \simeq 1$. In Methods we provide further details about spectral unfolding (which sets the local mean level spacing to unity, $\langle \varepsilon_{\alpha+1} - \varepsilon_{\alpha} \rangle = 1$), averaging $\langle \dots \rangle$ over disorder realizations, and a smooth filter $g(\varepsilon)$ to eliminate contributions of spectral edges. Of particular importance within the RMT is the result for the Gaussian orthogonal ensemble (GOE), $K_{\text{GOE}}(\tau) = 2\tau - \tau \ln(1 + 2\tau)$, applicable for systems with time-reversal symmetry [28].

Two important times characterize the SFF $K(\tau)$. We refer to those times as *scaled* times since they are extracted after the spectral unfolding. The first is the scaled Heisenberg time $\tau_{\text{H}} \equiv 1$ (see the vertical line in Fig. 1). It is the inverse mean level spacing for unfolded energy levels used in $K(\tau)$, and it is considered as the upper bound on physically relevant time scales in finite quantum systems. The second is the scaled Thouless time τ_{Th} , which is defined as the onset time of a linear ramp in $K(\tau)$ after which the SFF follows a universal RMT prediction, i.e., $K(\tau) \simeq K_{\text{GOE}}(\tau) \simeq 2\tau$ for $\tau > \tau_{\text{Th}}$ (see the open circles in Fig. 1). We define the system as quantum chaotic if $\tau_{\text{Th}}/\tau_{\text{H}} \rightarrow 0$ in the thermodynamic limit and consider the time regime $\tau \in [\tau_{\text{Th}}, \tau_{\text{H}}]$ as the regime of universal quantum chaotic dynamics.

A paradigmatic class of Hamiltonians that are expected to exhibit MBL are disordered spin chains with local, Heisenberg-like interactions and on-site

disorder,

$$\hat{H} = J_1 \sum_{\ell=1}^L (\hat{s}_{\ell}^x \hat{s}_{\ell+1}^x + \hat{s}_{\ell}^y \hat{s}_{\ell+1}^y + \Delta \hat{s}_{\ell}^z \hat{s}_{\ell+1}^z) \quad (2)$$

$$+ J_2 \sum_{\ell=1}^L (\hat{s}_{\ell}^x \hat{s}_{\ell+2}^x + \hat{s}_{\ell}^y \hat{s}_{\ell+2}^y + \Delta \hat{s}_{\ell}^z \hat{s}_{\ell+2}^z) + \sum_{\ell=1}^L w_{\ell} \hat{s}_{\ell}^z,$$

where \hat{s}_{ℓ}^{α} ($\alpha = x, y, z$) are spin-1/2 operators at site ℓ and L is the number of lattice sites. We use periodic boundary conditions, $\hat{s}_{\ell}^{\alpha} = \hat{s}_{L+\ell}^{\alpha}$, and consider the total spin projection $s^z = 0$ sector. We set $J_1 \equiv 1$ as the unit of energy. Disorder is introduced by independent and identically distributed local magnetic fields, with values $w_{\ell} \in [-W, W]$ drawn from a uniform distribution, and hence we refer to W as the disorder strength.

We study two models with disorder, the isotropic Heisenberg chain [$J_2 = 0$ and $\Delta = 1$ in equation (2)] and the anisotropic J_1 - J_2 chain [$J_2 = 1$ and $\Delta = 0.55$ in equation (2)]. While most of MBL studies focused on the first model, which is Bethe-ansatz integrable in the absence of disorder, we argue that it is more natural to study the possible breakdown of ergodicity in the J_1 - J_2 model, which in the absence of disorder is considered as a paradigmatic model to exhibit quantum chaos and eigenstate thermalization [4]. Hence more emphasis in our analysis is devoted to the J_1 - J_2 model, however our main results are valid for both models.

Examples of the SFF $K(\tau)$ in the J_1 - J_2 model at weak ($W=0.5$), moderate ($W=4$) and strong ($W=8$) disorder are shown in the main panel of Fig. 1. While the SFF takes into account spectral correlations at all energy scales, in the inset of Fig. 1 we also show results for the average level spacing ratio $\langle \tilde{r} \rangle$, which takes into account only the nearest energy levels and has been used as one of the central indicators for the emergence of MBL. The results are in agreement with expectations that the existence of a universal quantum chaotic regime in $K(\tau)$ is associated with $\langle \tilde{r} \rangle$ obeying the GOE predictions.

The main focus of our analysis is to extract the dependence of the Thouless time (in physical units, set by the energy J_1) on disorder W and system size L . To this end, we introduce the physical time t in Fig. 2a. We observe that the Thouless time t_{Th} , divided by the squared system size L^2 , yields perfect overlap of results for different system sizes for a wide range of W . The deviation at large W occurs when $t_{\text{Th}} \rightarrow t_{\text{H}}$ (see dashed lines in Fig. 2a, which denote t_{H}/L^2), where t_{H} is the Heisenberg time in physical units, which diverges exponentially fast with L (it is proportional to the inverse mean level spacing of

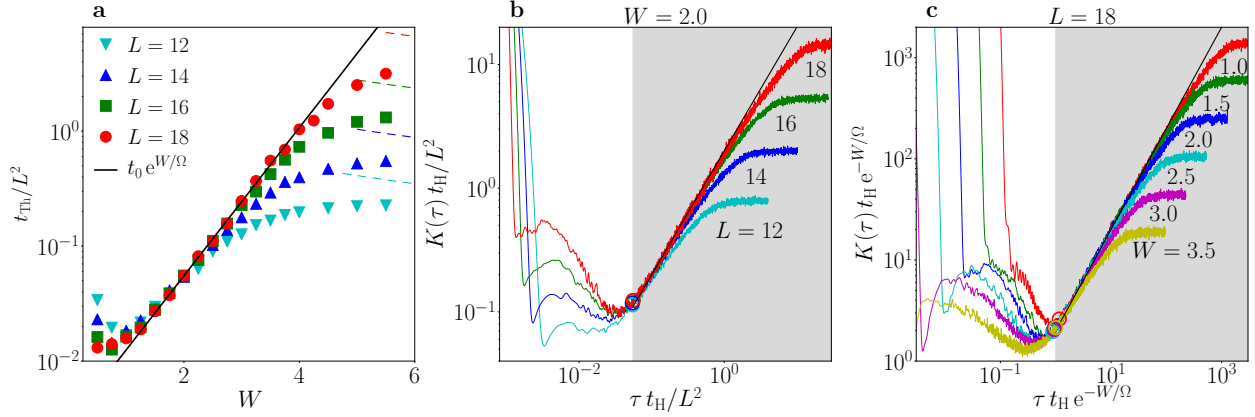


FIG. 2. **Thouless time t_{Th} extracted from the SFF $K(\tau)$.** Results in all panels are shown for the anisotropic J_1 - J_2 chain. **a**, Dependence of t_{Th}/L^2 on the disorder strength W , shown for four different lattices sizes L (see the legend). Physical time t is related to the scaled time τ as $\tau = t/t_{\text{H}}$, where the Heisenberg time t_{H} is defined as the inverse mean level spacing $t_{\text{H}} \equiv \hbar/\delta E$. [See Methods for the definition of δE ; we set $\hbar \equiv 1$.] Hence, the Thouless time (in physical units) is defined as $t_{\text{Th}} = \tau_{\text{Th}} t_{\text{H}}$, where τ_{Th} is extracted from $K(\tau)$ as shown in Fig. 1 and in Sec. S2 of the Supplementary Information. Solid line is a fit to $t_0 e^{W/\Omega}$ for $L = 18$ and $1.5 \leq W \leq 4$, with $t_0 = 2.84 \cdot 10^{-3}$ and $\Omega = 0.67$. Dashed lines denote the renormalized Heisenberg time t_{H}/L^2 . **b** and **c**, Renormalized SFF versus renormalized time. Shaded areas denote the regime of universal quantum chaotic dynamics, and open circles denote the renormalized Thouless time. Linear solid lines are the GOE results in the thermodynamic limit $K_{\text{GOE}}^\infty(\tau) \rightarrow 2\tau$. **b**, $K(\tau)t_{\text{H}}/L^2$ versus $\tau t_{\text{H}}/L^2$ at $W = 2$ and four different lattice sizes L . **c**, $K(\tau)t_{\text{H}}e^{-W/\Omega}$ versus $\tau t_{\text{H}}e^{-W/\Omega}$ at $L = 18$ and six different disorder strengths W .

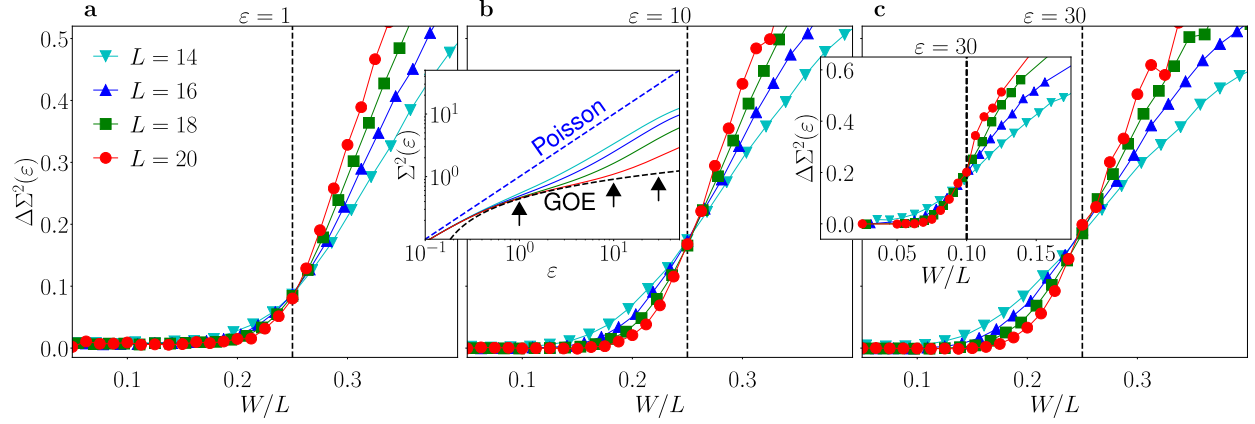


FIG. 3. **Number variance in disordered spin chains.** Results are shown for the anisotropic J_1 - J_2 chain in all panels except for the inset in **c**, where results for the isotropic Heisenberg chain are shown. The inset in **b** shows the number variance $\Sigma^2(\varepsilon)$ as a function of ε for the disorder strength $W = 4$ [see Methods for the definition of $\Sigma^2(\varepsilon)$]. The black and blue dashed lines in the inset denote the predictions for GOE, $\Sigma_{\text{GOE}}^2(\varepsilon) \simeq (2/\pi^2) (\ln(2\pi\varepsilon) + \gamma + 1 - \pi^2/8)$, where $\gamma \simeq 0.577$ is the Euler constant, and Poissonian spectrum, $\Sigma_{\text{Poisson}}^2(\varepsilon) = \varepsilon$. All the other results in panels **a**, **b** and **c**, respectively, display $\Delta\Sigma^2(\varepsilon) = [\Sigma^2(\varepsilon) - \Sigma_{\text{GOE}}^2(\varepsilon)] / [\Sigma_{\text{Poisson}}^2(\varepsilon) - \Sigma_{\text{GOE}}^2(\varepsilon)]$ at three different $\varepsilon = 1, 10, 30$. Those values of ε are denoted by arrows in the inset in **b**. Results are shown for different systems sizes L (see the legend) and are plotted versus renormalized disorder W/L . The vertical line in main panels is plotted at $W^*/L = 0.25$. The analysis of the SFF $K(\tau)$, which accounts for the noise in $K(\tau)$ and includes subleading terms to the expression in equation (4) [see Methods], gives $W^*/L \in [0.25, 0.27]$ at $L = 18$. The vertical line in the inset in **c** is plotted at $W^*/L = 0.10$.

energy levels). Another important observation from Fig. 2a is that the disorder only affects t_{Th} as a multiplicative factor, which increases exponentially with W . The solid line in Fig. 2a suggests that a very accurate double scaling of the Thouless time t_{Th} is given by

$$t_{\text{Th}} = t_0 e^{W/\Omega} L^2, \quad (3)$$

where t_0 is a characteristic time in units of \hbar/J_1 , and Ω is a constant. We verify equation (3) in Fig. 2b and c where, upon proper renormalization of both axes, the SFF $K(\tau)$ reveals a disorder- and system-size-independent onset of universal quantum chaotic dynamics.

Figure 2a provides a valuable insight for interpretation of results in finite systems. It shows that the deviation of t_{Th} from the function in equation (3) occurs in the same disorder regime for which $\langle \tilde{r} \rangle$ departs from the GOE prediction ($W \sim 4$ at $L = 18$; see also the inset of Fig. 1). Remarkably, this occurs because t_{Th} approaches the inverse mean level spacing set by t_{H} (which is a finite size effect), and not because of some transition to the MBL.

While for currently available system sizes ($L \lesssim 20$ using exact diagonalization) we can not verify the scaling of t_{Th} in equation (3) for very large W , we also see no indications of its breakdown. Assuming that the scaling (3) persists in strongly disordered regime, it suggests the emergence of quantum chaos for any finite disorder W since $t_{\text{Th}}/t_{\text{H}} \rightarrow 0$ in the thermodynamic limit $L \rightarrow \infty$ [see Methods for the scaling form of t_{H}]. In finite systems, one can assume the onset of effective MBL at disorder W^* that satisfies $t_{\text{Th}}(W^*) = t_{\text{H}}$, i.e., when features of the GOE energy spectral statistics disappear at all scales. This yields in the leading term

$$W^* \simeq \Omega \ln(2) L \propto L \quad (4)$$

and suggests the breakdown of MBL in the thermodynamic limit.

We check consistency of our observations with other measures for spectral correlations, such as the number variance $\Sigma^2(\varepsilon)$ and the average level spacing ratio $\langle \tilde{r} \rangle$. Figures 3 and 4, respectively, show the departure of $\Sigma^2(\varepsilon)$ and $\langle \tilde{r} \rangle$ from the GOE predictions in finite systems upon increasing disorder. Remarkably, the departure seems to consistently emerge at a fixed W/L , in agreement with equation (4).

In conclusion, a systematic analysis of the SFF provides a new perspective on quantum chaos and ergodicity in disordered systems. Approaching large disorder regime from the ergodic side, our results for the paradigmatic class of models expected to

exhibit MBL give no indications for the transition to the MBL. In fact, the observed clear scaling of the Thouless time suggests the emergence of quantum chaos for all disorder strengths. It is intriguing that our results carry analogies with numerical studies of quantum chaos in homogeneous systems with weak integrability breaking perturbations [29]: in that case, manifestations of quantum chaos extend to smaller perturbations with increasing the system size, eventually extending to all nonzero perturbations in the thermodynamic limit. Understanding the boundaries of applicability of quantum chaos, as

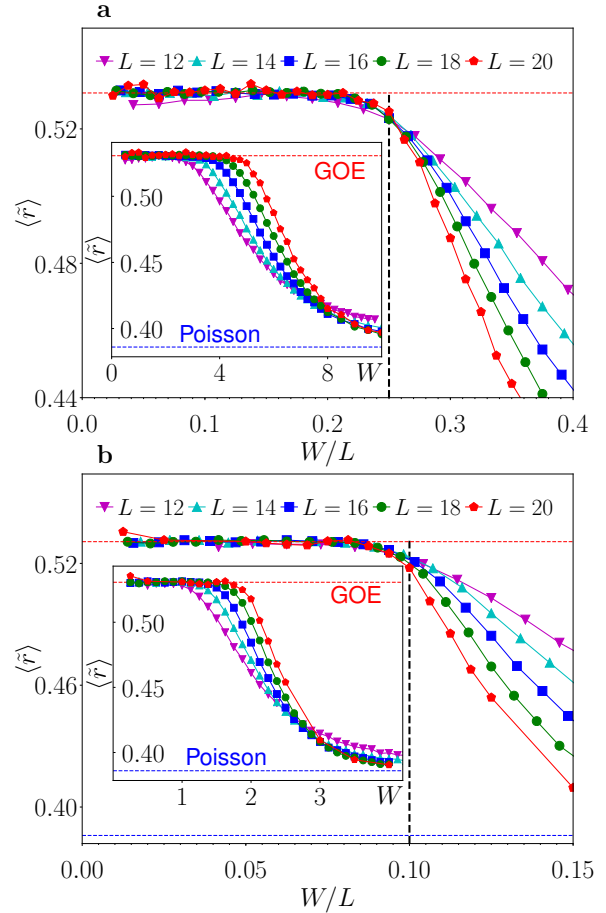


FIG. 4. **Average level spacing ratio $\langle \tilde{r} \rangle$ in disordered spin chains.** a, Anisotropic J_1 - J_2 chain. b, Isotropic Heisenberg chain. In the main panels we show $\langle \tilde{r} \rangle$ for different systems sizes L (see the legend) as a function of renormalized disorder W/L . Vertical lines are identical to the vertical lines in Fig. 3. In the insets we show $\langle \tilde{r} \rangle$ for different systems sizes L as a function of disorder W without renormalization.

well as to develop analytical techniques for its studies in generic many-body systems away from perturbative regimes, represent an outstanding problem for future research. Another challenge is to better understand implications of our results for transport properties. While the exponential scaling of Thouless times with disorder strength is consistent with observations of exponentially small dc conductivity [30], there is a natural question whether the onset of universal quantum chaotic dynamics at the Thouless time is associated with a crossover from subdiffusive to diffusive transport.

METHODS

A. Spectral form factor.

In the definition of the SFF $K(\tau)$ in equation (1) we included a filtering function $g(\varepsilon_\alpha)$ to avoid boundary effects. Its specific form should not influence the main features of $K(\tau)$, provided that the filtering function is smooth enough (e.g. analytic), symmetric w.r.t. the centre of the unfolded spectrum, and has a vanishingly small amplitude at the spectral edges. In our calculations we first perform spectral unfolding (see below) for each disorder realization separately. Then we filter each unfolded spectrum using a Gaussian filter $g(\varepsilon_\alpha) = \exp\{-\frac{(\varepsilon_\alpha - \bar{\varepsilon})^2}{2(\eta\Gamma)^2}\}$, where $\bar{\varepsilon}$ and Γ^2 are the average energy and the variance, respectively, at a given disorder realization, and η a dimensionless parameter that controls the effective fraction of eigenstates included in $K(\tau)$. We set $\eta = 0.5$ in the calculations presented in Fig. 1 and 2. To ensure proper normalization, yielding $K(t \gg 1) \simeq 1$ in general and $K(t) \equiv 1$ for Poisson random spectrum, we then set $Z = \langle \sum_\alpha |g(\varepsilon_\alpha)|^2 \rangle$.

B. Spectral unfolding.

We eliminate the influence of the local density of states by spectral unfolding. It transforms an ordered set of Hamiltonian eigenvalues $\{E_\alpha\}$ to an ordered set of unfolded eigenvalues $\{\varepsilon_\alpha\}$. Following the standard unfolding procedure, we introduce the cumulative spectral function $\mathcal{G}(E) = \sum_\alpha \Theta(E - E_\alpha)$, where Θ is the unit step function. The step-wise distribution function is then smoothed out by fitting a polynomial $g_n(E)$ of degree n to $\mathcal{G}(E)$ and the unfolded eigenvalues are defined as $\varepsilon_\alpha = g_n(E_\alpha)$.

We verified that using polynomials $g_n(E)$ of different degrees n in the unfolding procedure does not affect the final results. We used spectral unfolding with $n = 10$ in calculations of the SFF $K(\tau)$ and $n = 3$ in calculations of the level number variance $\Sigma^2(\varepsilon)$, where smaller spectral samples were used, see Methods E.

C. Level spacing ratio and number variance.

In the inset of Fig. 1 and in Fig. 4 we study properties of the level spacing ratio

$$\tilde{r}_\alpha = \frac{\min\{\delta E_\alpha, \delta E_{\alpha-1}\}}{\max\{\delta E_\alpha, \delta E_{\alpha-1}\}} = \min\{r_\alpha, r_\alpha^{-1}\}, \quad (5)$$

which is, for a target eigenstate $|\alpha\rangle$, defined through the quantity $r_\alpha = \delta E_\alpha / \delta E_{\alpha-1}$. Here, r_α is the ratio of two consecutive energy level spacings $\delta E_\alpha = E_{\alpha+1} - E_\alpha$. Hence, no unfolding is necessary to eliminate the influence of finite-size effects through the local density of states. We obtain the average level spacing ratio $\langle \tilde{r} \rangle$ by first averaging over $N_{\text{ev}} = 500$ eigenstates near the centre of the spectrum for every disorder realization, and then over an ensemble of spectra for different disorder realizations. Numerical results are compared to the well-known results within the random matrix theory [31], namely the GOE prediction $\tilde{r}_{\text{GOE}} \approx 0.5307$ and the prediction for energy levels with Poisson statistics $\tilde{r}_{\text{Poisson}} \approx 0.3863$.

In Fig. 3 we study the level number variance, which is defined as the variance of the number of unfolded levels $N(\varepsilon)$ within an energy interval of width ε , specified in the units of the mean level spacing:

$$\Sigma^2(\varepsilon) = \langle N^2(\varepsilon) \rangle - \langle N(\varepsilon) \rangle^2. \quad (6)$$

Since the mean level spacing equals unity in an unfolded spectrum, one has $\langle N(\varepsilon) \rangle = \varepsilon$ and hence the energy parameter in equation (6) can be replaced by the average number of levels $\langle N \rangle$.

Note that $\Sigma^2(\varepsilon)$ is a non-local integral transform of $K(\tau)$ [28], hence it is still a pure two-point function, while $\langle \tilde{r} \rangle$ can in general be expressed in terms of multi-point spectral correlations.

D. Thouless time versus Heisenberg time.

In Fig. 2a we calculate the Thouless time t_{Th} in physical units. To this end, we first introduce the mean level spacing $\overline{\delta E} = \Gamma_0 / (\chi \mathcal{D})$,

where $\Gamma_0^2 = \langle \text{Tr}\{\hat{H}^2\} \rangle / \mathcal{D} - \langle \text{Tr}\{\hat{H}\} \rangle^2 / \mathcal{D}^2$ is the variance after disorder averaging and χ controls the number of energy levels in the interval $[\bar{E}, \bar{E} + \Gamma_0]$, with $\bar{E} = \langle \text{Tr}\{\hat{H}\} \rangle / \mathcal{D}$. We calculate Γ_0^2 in the grand canonical ensemble, which yields $\Gamma_0^2 = L[(1 + J_2^2)/8 + (\Delta^2 + (J_2\Delta)^2)/16 + W^2/12]$, and we calculate χ using the Gaussian approximation for the density of states, which yields $\chi = \int_0^{\Gamma_0} \exp\{-E^2/(2\Gamma_0^2)\} / (\sqrt{2\pi}\Gamma_0) dE = (1/2)\text{erf}[1/\sqrt{2}] \approx 0.3413$.

The Heisenberg time t_H in physical units is defined through the inverse mean level spacing as $t_H = \hbar/\delta E$ (we set $\hbar \equiv 1$). Using the expression for t_{Th} in equation (3), and the Stirling's approximation for the Hilbert space dimension $\mathcal{D} = \binom{L}{L/2} \simeq \sqrt{2/\pi} \exp\{L \ln 2\} / \sqrt{L}$, the equality $t_{Th}(W^*) = t_H$ implies

$$\chi^{-1} \sqrt{\frac{\pi}{2}} t_0 \Gamma_0 L^{5/2} e^{W^*/\Omega} = e^{L \ln 2}. \quad (7)$$

Since there are terms on both sides of the equation that increase exponentially, the leading term of the solution gives $W^* \simeq \Omega \ln(2)L$, which is the result in equation (4). In finite systems with $L \lesssim 20$, however, subleading terms are noticeable and equation (7) needs to be solved numerically for quantitative comparisons. We first note that the determination of the scaled Thouless time τ_{Th} from the SFF $K(\tau)$ in finite systems is not sharply defined due to a noise in $K(\tau)$ when it approaches $K_{GOE}(\tau)$. In Supplementary Information we carry out an extrapolation analysis, which suggests that our τ_{Th} in general underestimates the extrapolated Thouless time $\tilde{\tau}_{Th}$ by a constant factor, which is very conservatively estimated to be between 2 and 4. We hence replace $t_0 \rightarrow \tilde{t}_0$ in equation (7) and solve it for $\tilde{t}_0 \in [2t_0, 4t_0]$,

which at $L = 18$ yields $W^*/L \in [0.25, 0.27]$, in excellent quantitative agreement with results in Fig. 3 and 4.

E. Numerical implementation.

Energy spectra used in the $K(\tau)$ calculations shown in Fig. 1 and 2 were obtained by means of full numerical diagonalization. For systems smaller than $L = 18$, diagonalization has been performed for $N_{\text{samples}} = 1000$ different disorder realizations, for each value of W and L . In the $L = 18$ case, the spectra have been calculated for 400 different disorder realizations.

In studies of $\Sigma^2(\varepsilon)$ and $\langle \tilde{r} \rangle$, shown in Fig. 3 and 4, respectively, we used the shift-and-invert diagonalization algorithm [32], with which we calculated $n_{\text{ev}} = 500$ eigenvalues near the centre of the spectra. This approach enabled us to study systems up to size $L = 20$ as opposed to the $L = 18$ in the full diagonalization case. Using shift-and-invert approach, 1000 disorder realizations have been performed for smaller systems and 200 disorder realizations were used for the $L = 20$ system.

ACKNOWLEDGMENTS

We acknowledge insightful discussions with W. De Roeck, F. Heidrich-Meisner, D. Luitz, A. Polkovnikov, P. Prelovšek, M. Rigol, T. H. Seligman and M. Žnidarič. This work was supported by the Slovenian Research Agency (ARRS), Research Core Fundings No. P1-0044 and No. P1-0402, and by European Research Council (ERC) under Advanced Grant 694544 – OMNES.

-
- [1] D. Basko, I. Aleiner, and B. Altshuler, Metal-insulator transition in a weakly interacting many-electron system with localized single-particle states, *Ann. Phys.* **321**, 1126 (2006).
 - [2] V. Oganesyan and D. A. Huse, Localization of interacting fermions at high temperature, *Phys. Rev. B* **75**, 155111 (2007).
 - [3] P. W. Anderson, Absence of diffusion in certain random lattices, *Phys. Rev.* **109**, 1492 (1958).
 - [4] L. D'Alessio, Y. Kafri, A. Polkovnikov, and M. Rigol, From quantum chaos and eigenstate thermalization to statistical mechanics and thermodynamics, *Adv. Phys.* **65**, 239 (2016).
 - [5] J. Eisert, M. Friesdorf, and C. Gogolin, Quantum many-body systems out of equilibrium, *Nature Phys.* **11**, 124 (2015).
 - [6] G. Casati, F. Valz-Gris, and I. Guarneri, On the connection between quantization of nonintegrable systems and statistical theory of spectra, *Lettere al Nuovo Cimento* **28**, 279 (1980).
 - [7] O. Bohigas, M. J. Giannoni, and C. Schmit, Characterization of chaotic quantum spectra and universality of level fluctuation laws, *Phys. Rev. Lett.* **52**, 1 (1984).
 - [8] M. V. Berry, Semiclassical theory of spectral rigidity, *Proc. R. Soc. Lond. A* **400**, 229 (1985).

- [9] J. S. Cotler, G. Gur-Ari, M. Hanada, J. Polchinski, P. Saad, S. H. Shenker, D. Stanford, A. Streicher, and M. Tezuka, Black holes and random matrices, *JHEP* **5** (2017), 118.
- [10] J. Cotler, N. Hunter-Jones, J. Liu, and B. Yoshida, Chaos, complexity, and random matrices, *JHEP* **11** (2017), 48.
- [11] H. Gharibyan, M. Hanada, S. H. Shenker, and M. Tezuka, Onset of random matrix behavior in scrambling systems, *JHEP* **7** (2018), 124.
- [12] X. Chen and A. W. W. Ludwig, Universal spectral correlations in the chaotic wave function and the development of quantum chaos, *Phys. Rev. B* **98**, 064309 (2018).
- [13] G. Montambaux, D. Poilblanc, J. Bellissard, and C. Sire, Quantum chaos in spin-fermion models, *Phys. Rev. Lett.* **70**, 497 (1993).
- [14] T. Prosen, Ergodic properties of a generic nonintegrable quantum many-body system in the thermodynamic limit, *Phys. Rev. E* **60**, 3949 (1999).
- [15] L. F. Santos and M. Rigol, Onset of quantum chaos in one-dimensional bosonic and fermionic systems and its relation to thermalization, *Phys. Rev. E* **81**, 036206 (2010).
- [16] B. Bertini, P. Kos, and T. Prosen, Exact spectral form factor in a minimal model of many-body quantum chaos, *Phys. Rev. Lett.* **121**, 264101 (2018).
- [17] D. J. Luitz, N. Laflorencie, and F. Alet, Many-body localization edge in the random-field Heisenberg chain, *Phys. Rev. B* **91**, 081103 (2015).
- [18] R. Nandkishore and D. A. Huse, Many-body localization and thermalization in quantum statistical mechanics, *Ann. Rev. Cond. Mat. Phys.* **6**, 15 (2015).
- [19] E. Altman and R. Vosk, Universal dynamics and renormalization in many-body-localized systems, *Ann. Rev. Cond. Mat. Phys.* **6**, 383 (2015).
- [20] J. Z. Imbrie, On many-body localization for quantum spin chains, *J. Stat. Phys.* **163**, 998 (2016).
- [21] M. Serbyn, Z. Papić, and D. A. Abanin, Local conservation laws and the structure of the many-body localized states, *Phys. Rev. Lett.* **111**, 127201 (2013).
- [22] V. Ros, M. Müller, and A. Scardicchio, Integrals of motion in the many-body localized phase, *Nuc. Phys. B* **891**, 420 (2015).
- [23] M. Schreiber, S. S. Hodgman, P. Bordia, H. P. Lüschen, M. H. Fischer, R. Vosk, E. Altman, U. Schneider, and I. Bloch, Observation of many-body localization of interacting fermions in a quasi-random optical lattice, *Science* **349**, 842 (2015).
- [24] J. Smith, A. Lee, P. Richerme, B. Neyenhuis, P. W. Hess, P. Hauke, M. Heyl, D. A. Huse, and C. Monroe, Many-body localization in a quantum simulator with programmable random disorder, *Nat. Phys.* **12**, 907 (2016).
- [25] D. J. Luitz, F. Huveneers, and W. De Roeck, How a small quantum bath can thermalize long localized chains, *Phys. Rev. Lett.* **119**, 150602 (2017).
- [26] M. Žnidarič and M. Ljubotina, Interaction instability of localization in quasiperiodic systems, *Proc. Natl. Acad. Sci.* **115**, 4595 (2018).
- [27] W. De Roeck and F. Huveneers, Stability and instability towards delocalization in many-body localization systems, *Phys. Rev. B* **95**, 155129 (2017).
- [28] M. L. Mehta, *Random Matrices and the Statistical Theory of Spectra*, 2nd ed. (Academic, New York, 1991).
- [29] R. Mondaini and M. Rigol, Eigenstate thermalization in the two-dimensional transverse field Ising model. II. Off-diagonal matrix elements of observables, *Phys. Rev. E* **96**, 012157 (2017).
- [30] O. S. Barišić and P. Prelovšek, Conductivity in a disordered one-dimensional system of interacting fermions, *Phys. Rev. B* **82**, 161106 (2010).
- [31] Y. Y. Atas, E. Bogomolny, O. Giraud, and G. Roux, Distribution of the ratio of consecutive level spacings in random matrix ensembles, *Phys. Rev. Lett.* **110**, 084101 (2013).
- [32] F. Pietracaprina, N. Macé, D. J. Luitz, and F. Alet, Shift-invert diagonalization of large many-body localizing spin chains, *SciPost Phys.* **5**, 045 (2018).

Supplementary Information: Quantum chaos challenges many-body localization

Jan Šuntajs,¹ Janez Bonča,^{1,2} Tomaž Prosen², and Lev Vidmar¹

¹*Department of Theoretical Physics, J. Stefan Institute, SI-1000 Ljubljana, Slovenia*

²*Department of Physics, University of Ljubljana, SI-1000 Ljubljana, Slovenia*

IMPLEMENTATION OF THE SPECTRAL FORM FACTOR (SFF)

The results of our calculations of the SFF $K(\tau)$, shown in Fig. 1 and 2, were calculated according to equation (1) in the main text. We also compare the SFF $K(\tau)$ with the *connected* SFF, $K_c(\tau)$. The latter is obtained by subtracting a nonuniversal disconnected part from $K(\tau)$,

$$K_c(\tau) = \frac{1}{Z} \left(\left\langle \left| \sum_{\alpha=1}^{\mathcal{D}} g(\varepsilon_{\alpha}) e^{-i\varepsilon_{\alpha}\tau} \right|^2 \right\rangle - \frac{A}{B} \left| \left\langle \sum_{\alpha=1}^{\mathcal{D}} g(\varepsilon_{\alpha}) e^{-i\varepsilon_{\alpha}\tau} \right\rangle \right|^2 \right), \quad (\text{S1})$$

where A and B are the normalization constants ensuring the vanishing of $K_c(\tau)$ in the $\tau \rightarrow 0$ limit, accounting for the spectral filtering

$$A = \left\langle \left| \sum_{\alpha=1}^{\mathcal{D}} g(\varepsilon_{\alpha}) \right|^2 \right\rangle, \quad B = \left| \left\langle \sum_{\alpha=1}^{\mathcal{D}} g(\varepsilon_{\alpha}) \right\rangle \right|^2. \quad (\text{S2})$$

The goal of this section is to analyze the difference between $K(\tau)$ and $K_c(\tau)$ for determining the Thouless time, as well as the influence of the spectral filtering $g(\varepsilon)$. All the results correspond to the disordered anisotropic J_1 - J_2 chain. An example of the results for the system size $L = 18$ and disorder strength $W = 1$ is shown in Fig. S1. While the short time nonuniversal behaviour of $K_c(\tau)$ and $K(\tau)$ [cf. Fig. S1a and b, respectively] is clearly different, they both follow the GOE prediction $K_{\text{GOE}}(\tau)$ after the scaled Thouless time τ_{Th} . The open circles in Fig. S1 denote τ_{Th} , which is almost identical for $K_c(\tau)$ and $K(\tau)$.

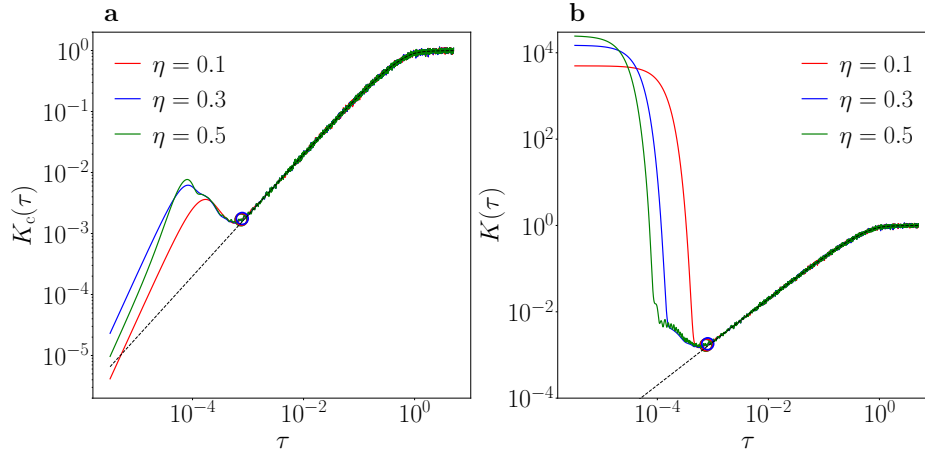


FIG. S1. **Comparison between a connected and unconnected SFF, using different spectral filters.** **a**, The connected SFF $K_c(\tau)$, defined in equation (S1). **b**, The SFF $K(\tau)$, defined in equation (1) in the main text. We use a Gaussian spectral filter $g(\varepsilon)$, defined in Methods, where η determines the effective width of the filter. Here we compare results for $\eta = 0.1, 0.3$ and 0.5 . Open circles denote the scaled Thouless time τ_{Th} . Results are shown for the system size $L = 18$ and disorder strength $W = 1$.

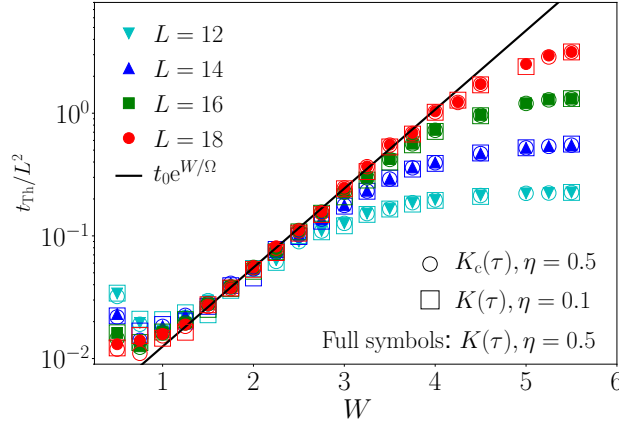


FIG. S2. **Comparison of Thouless times extracted from different implementations of the SFF $K(\tau)$.** We show the Thouless time t_{Th} , divided by the squared system size L^2 , as a function of disorder strength W . We obtain Thouless times t_{Th} from scaled Thouless times τ_{Th} as $t_{\text{Th}} = \tau_{\text{Th}} t_{\text{H}}$, as in the main text. Filled symbols and the solid line are identical to the results in Fig. 2a in the main text. Open squares are results for t_{Th} extracted from $K(\tau)$ using the Gaussian spectral filter with the width $\eta = 0.1$. Open circles are results for t_{Th} extracted from the connected SFF $K_c(\tau)$ with $\eta = 0.5$.

In Fig. S1 we also show results for different widths η of a Gaussian spectral filter $g(\varepsilon)$, defined in Methods. Results for τ_{Th} appear to be fairly independent of the width η of the Gaussian filter used in our calculations. Note, however, that $\eta \lesssim 0.5$ is needed to eliminate contributions from eigenstates at the spectral edges. Since, in general, one wishes to include as many eigenstates as possible in the analysis, we find that setting $\eta = 0.5$ is the optimal parameter choice of the Gaussian spectral filtering.

Results for the Thouless times t_{Th} are systematically analyzed in Fig. S2. We compare t_{Th} extracted from three different implementations of the SFF, using: (i) $K(\tau)$ with the Gaussian spectral filter with the width $\eta = 0.5$, used also in the main text [filled symbols in Fig. S2]; (ii) $K(\tau)$ with $\eta = 0.1$ [open squares in Fig. S2]; and (iii) the connected $K_c(\tau)$ with $\eta = 0.5$ [open circles in Fig. S2]. The excellent agreement between results using different implementations of the SFF suggest robustness of the scaling of t_{Th} , reported in equation (3) in the main text, which is one of our main results.

EXTRACTION OF THOULESS TIMES FROM THE SFF

Here we describe the protocol to extract the scaled Thouless time τ_{Th} from the SFF $K(\tau)$. [An analogous procedure is applied for the connected SFF $K_c(\tau)$]. Each $K(\tau)$ curve is calculated for 5000 times τ_i in the window $\tau_i \in [1/(2\pi\mathcal{D}), 5]$, with τ_i being equidistant in logarithmic scale. As a first step, we smoothen out random fluctuations in $K(\tau)$ by calculating a running mean such that each new $K(\tau_i)$ is the average over 100 nearest values of $K(\tau_i)$, and hence the final number of data points is reduced to 4901. As a second step, we analyze the difference between $K(\tau)$ and the GOE prediction $K_{\text{GOE}}(\tau) = 2\tau - \tau \ln(1 + 2\tau)$. We introduce the deviation measure

$$\Delta K(\tau) = \left| \log \frac{K(\tau)}{K_{\text{GOE}}(\tau)} \right| \quad (\text{S3})$$

and define the scaled Thouless time τ_{Th} as the time at which $\Delta K(\tau)$ becomes smaller than some threshold value ϵ . We use $\epsilon = 0.05$ for all results shown in the paper.

Figure S3 illustrates the protocol to extract τ_{Th} for the disordered anisotropic J_1 - J_2 chain. We show results at $L = 18$ for different disorders $W = 1, 3, 4$ and different widths $\eta = 0.1, 0.3, 0.5$ of the Gaussian filter $g(\varepsilon)$,

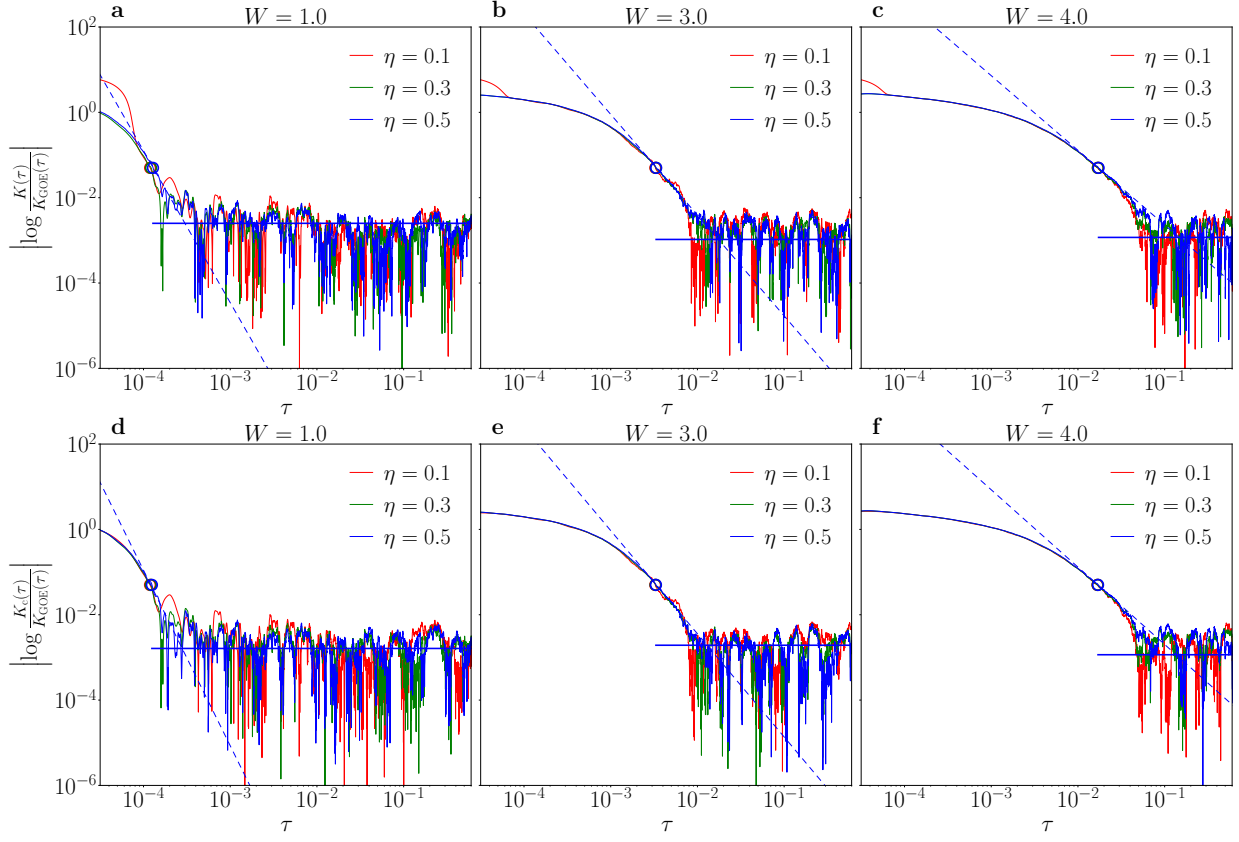


FIG. S3. **Extraction of the Thouless time.** In the upper row (panels **a**, **b** and **c**) we plot the deviation measure $\Delta K(\tau)$ from equation (S3) to quantify the difference between the SFF $K(\tau)$ and the GOE prediction $K_{\text{GOE}}(\tau)$. The lower row (panels **d**, **e** and **f**) shows the analogous quantity for the connected SFF $K_c(\tau)$. Results are shown for the anisotropic J_1 - J_2 chain with the disorder strengths $W = 1$ (panels **a** and **d**), $W = 3$ (panels **b** and **e**) and $W = 4$ (panels **c** and **f**). In all panels we show results for three different widths $\eta = 0.1, 0.3, 0.5$ of the Gaussian filter $g(\varepsilon)$. Circles denote the scaled Thouless time τ_{Th} . Horizontal solid lines are the averages over the noisy data at $\tau \gg \tau_{\text{Th}}$ and dashed lines are tangents to $K(\tau)$ at $\tau = \tau_{\text{Th}}$.

for both unconnected and connected SFF (upper and lower row in Fig. S3, respectively). The agreement of $K(\tau)$ with $K_{\text{GOE}}(\tau)$ in finite systems is associated with the emergence of noisy data in $\Delta K(\tau)$, with $\Delta K(\tau) \ll 1$. We choose τ_{Th} (see the circles in Fig. S3) such that $\Delta K(\tau_{\text{Th}})$ is larger than the noise. However, such choice slightly underestimates τ_{Th} . We estimate the correction by a linear extrapolation of $\Delta K(\tau)$ at $\tau = \tau_{\text{Th}}$ to the regime of noisy data (see the solid and dashed lines in Fig. S3). A conservative estimate yields a corrected Thouless time $\tilde{\tau}_{\text{Th}} \in [2\tau_{\text{Th}}, 4\tau_{\text{Th}}]$, which is then used in Methods to get quantitative predictions for W^*/L at system sizes of the order $L \lesssim 20$.